Master of Science Thesis

The effect of fluid additives on the compaction creep of sand aggregates and sandstone cylinders

Eva Hollebeek

Utrecht University, Faculty of Geosciences, Department of Earth Sciences
March 2012

Supervisors: Prof. Dr. C.J. Spiers and MSc. A. Pluymakers

Universiteit Utrecht

Table of contents

Abstract 3

1. Introduction 4

2.1. Experimental method – Uniaxial compaction creep experiments 4
2.1.1. Starting material and sample preparation 5
2.1.2. Experimental set-up 5
2.1.3. Testing procedure 6
2.1.4. Data processing and error analysis 7
2.2. Experimental method – Stress relaxation experiments 8
2.2.1. Starting material and sample preparation 8
2.2.2. Experimental set-up 11
2.2.3. Testing procedure 11
2.2.4. Data processing and error analysis 11

3.1. Results of uniaxial compaction creep experiments 12
3.1.1. Dry experiments 12
3.1.2. Wet experiments 13
3.1.3. Effect of temperature on compaction creep 13
3.2. Results of stress relaxation experiments 17
3.2.1. Bentheim samples 17
3.2.2. Fontainebleau samples 19

4.1. Discussion of uniaxial compaction creep experiments 21
4.1.1. Deformation mechanism 21
4.1.2. Effect of pH 22
4.1.3. Effect of impurities on quartz dissolution and fracturing 23
4.1.4. Effect of saturated silica solution 25
4.1.5. Effect of Temperature 25
4.2. Discussion of stress relaxation experiments 25
4.2.1. Bentheim experiments 26
4.2.2. Fontainebleau experiments 26

5. Conclusions 28

Acknowledgements 28
Appendix I 29
References 29

Abstract
Compaction creep of reservoir rocks causes surface subsidence above producing oil and gas fields worldwide. To investigate if compaction creep could be restricted both uniaxial compaction and triaxial stress relaxation experiments are performed on sand aggregates (Beaujean) and sandstone cylinders (Bentheim and Fontainebleau) respectively. Different pore fluids were tested for their effect on compaction creep, namely distilled water, aluminium chloride solution (0.1 M and 0.01 M), sodium chloride solution (0.3 M), sodium sulfate solution (0.15 M), sodium silicate solution (silica saturated solution) and lab air (i.e. dry). The uniaxial compaction experiments were performed in constant stress mode both at room temperature and 80˚C. The stress relaxation experiments were performed at 80˚C. All samples showed creep deformation. The main compaction deformation mechanism for wet Beaujean sand and Bentheim sandstone was inferred to be fluid enhanced microcracking, which was inhibited by aluminium chloride and by sodium silicate. Creep was enhanced by sodium chloride and by sodium sulfate. The results are in line with the known effects of pH and the presence of sodium or aluminium ions on stress corrosion cracking. The stress relaxation experiments on Fontainebleau sandstone did not deliver consistent results; further research is required on this material.

1. Introduction

Extraction of hydrocarbons leads to reservoir rock compaction, which results in ongoing subsidence at oil and gas fields worldwide. Well-known examples of locations where hydrocarbon extraction leads to surface subsidence are; Goose Creek (South Carolina, USA), Niigata (Japan), Bolivar Coast (Texas, USA) and Groningen (The Netherlands) (de Waal and Smits, 1988). Very little is known about the factors controlling ongoing subsidence, even though compaction and subsequent subsidence have environmental, technical and financial consequences. Associated problems include damage to buildings, induced seismicity, possible flooding of coastal areas and the effects on flow direction of surface and ground water.

For a better understanding of ongoing subsidence, the compaction creep of reservoir rocks has to be investigated. Previous research has been done on sandstone cylinders (e.g. Klein et al., 2001; Hettema et al., 1998), on sand aggregates and on loose sand grains (e.g. Brzesowsky, 1995, Karner et al., 2005, Hangx et al., 2010). Microstructural studies and acoustic emission experiments have shown that grain failure by (subcritical) microcracking plus grain rearrangements are the main mechanisms of creep deformation when pressure and temperature are low (i.e. under shallow conditions) (Atkinson, 1979). Dissolution processes seem to be not of importance (Hangx et al., 2010 and Chester et al., 2005). The processes of microcracking and thus of compaction can either be enhanced or inhibited by the addition of chemically active fluids (Dove, 1995; Hangx et al., 2010; Atkinson, 1979). These coupled chemical-mechanical creep effects are expected to depend on factors such as pore fluid pH, grain size, temperature and effective stress (Atkinson, 1979; Schutjens, 1991). Hangx et al. (2010) tested the effect of CO_2 on compaction creep and found that adding dissolved CO_2 significantly decreases compaction creep by subcritical grain cracking, whereas Brzesowsky et al. (1994) have determined that adding sodium chloride significantly increases compaction creep of sand aggregates, by this mechanism.

The aim of the present study is to contribute to the better understanding and possibility to mitigation of sandstone creep by finding a suitable additive which will inhibit compaction creep and therefore the amount of subsidence, above depleted sandstone reservoirs. To this end, we performed uniaxial compaction creep experiments on sand aggregates and triaxial stress relaxation experiments on sandstone cylinders, with use of different fluids. Pore fluids tested during the stress relaxation experiments include distilled water, aluminium chloride and lab air. Additionally solutions of sodium chloride, sodium sulfate and sodium silicate were used for the compaction creep experiments. Also we have investigated the effect of temperature, by performing the compaction creep experiments on both room temperature and 80˚C. The stress relaxation experiments were done at 80˚C only.

2.1 Experimental method – Uniaxial compaction creep experiments

We conducted a series of fixed-load, uniaxial compaction experiments on quartz sand aggregates, in which we investigated the effect of chemical environment. We used aqueous solutions containing different concentrations of aluminium chloride, sodium chloride, sodium sulfate and sodium silicate, as well as pure distilled water and lab air (i.e. dry experiment) (see Table 1).

2.1.1. Starting material and sample preparation

The quartz sand used in the present experiments was obtained from the Heksenberg Formation exposed in the Beaujean quarry near Heerlen, The Netherlands. The material was sieved into a range of 100 μm – 480 μm by former workers. The grain size distribution determined using a Malvern particle sizer is plotted in Figure 1. The most frequent grainsize ranges between 220 and 350 μm. The pore fluids used during the experiments were distilled water, aluminium chloride solution, several sodium solutions and a saturated silica solution. For the solutions containing aluminium we dissolved $AlCl_3*6H_2O$ in concentrations of 0.1 M and 0.01 M. To create the sodium solutions NaCl and Na_2SO_4 were dissolved. Molarities of respectively 0.3 M and 0.15 M were used for the NaCl and Na_2SO_4 solutions to have similar chloride and sodium concentrations to the 0.1 M aluminium chloride and the sodium chloride solutions respectively. To create the silica saturated solution NaSi is dissolved to a solution containing 0.27% SiO_2, in percentage of total solution. This produces a silica saturated solution (Iler 1979).

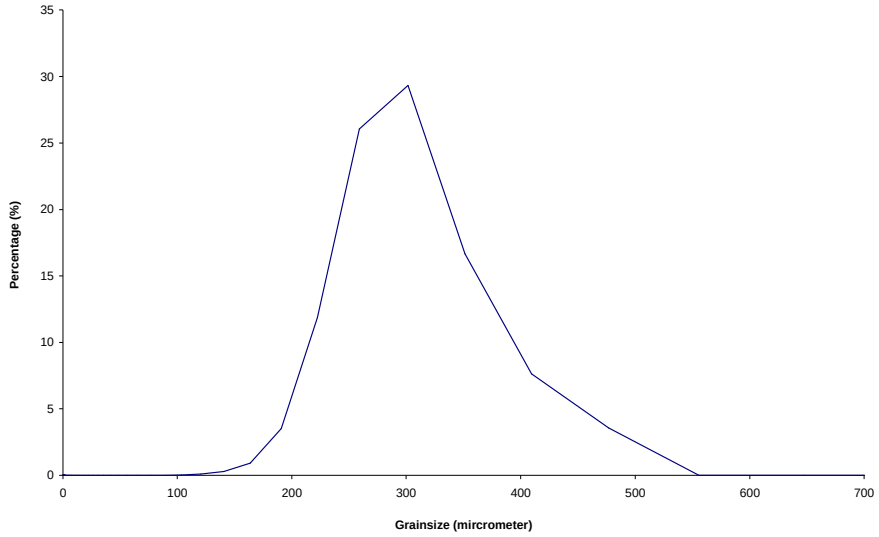

Figure 1: Grain size distribution of the sieved fraction of Beaujean sand used.

2.1.2. Experimental set-up

The compaction experiments were performed on sand aggregates using an uniaxial compaction vessel (hardened stainless steel, Remanit – 4122) located in an Instron 8562 loading frame equipped with a 100 kN load cell (accuracy 0.1%); see Figure 2. The diameter of the vessel is 19.18 mm. To attain a cylindrical sample with 1:1 sample length to sample diameter ratio, 8.84 g quartz sand was used for the experiments assuming a starting porosity of approximately 39 %. The pistons are equipped with Viton-O-ring seals. Fluid was inserted in the vessel via a central bore hole in the top piston. A porous plate was present at the tip of both bottom and top piston to prevent sand grains from entering the piston bore. During the experiment the fluid inlet was left open to the atmosphere so fluid was at ambient pressure conditions. For experiments at elevated temperatures the vessel and its content were heated by an external furnace to a temperature of 80°C, controlled by a Eurotherm temperature controller (resolution within 0.5°C). Sample temperature was measured by a thermocouple embedded in the vessel wall adjacent to the sample at a central height. Displacement was measured both using the Linear Variable Differential Transducer (LVDT) located in the Instron drive unit, and an external Sangamo LVDT with a range of 1.2 mm and a resolution

of 0.05%. The Sangamo LVDT measures relative displacement between the piston and the top part of the main vessel during the compaction tests (see Figure 2).

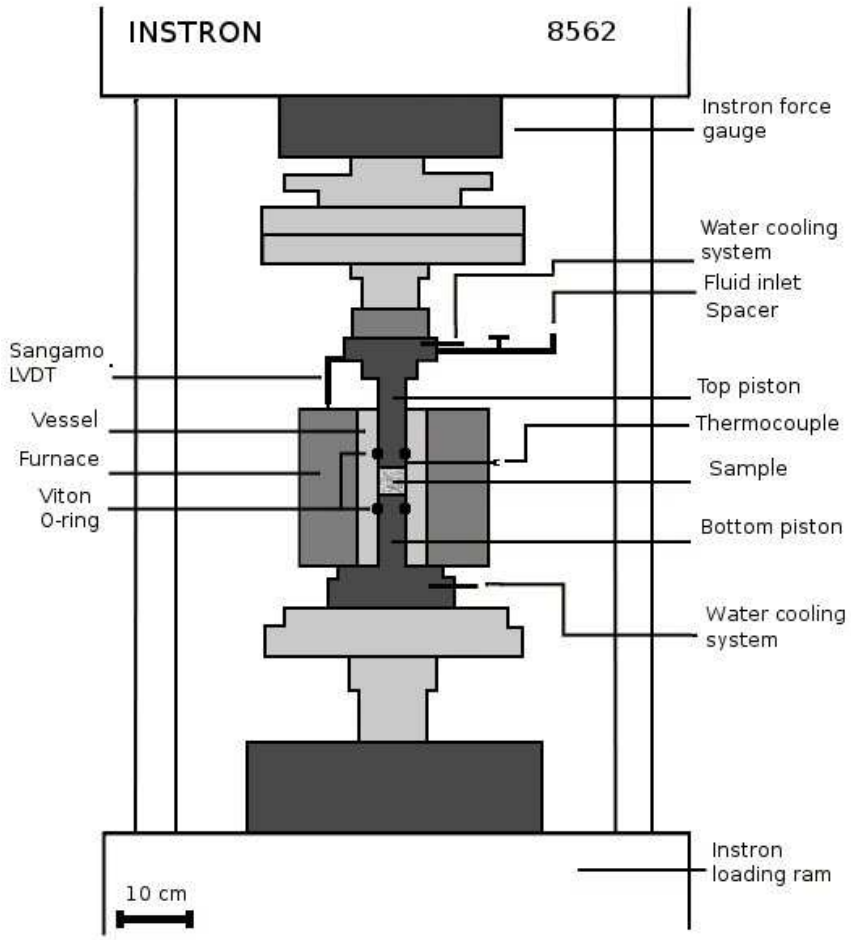

Figure 2: Schematic diagram showing the uniaxial compaction vessel in the Instron loading frame.

2.1.3. Testing procedure

The experiments were performed under the conditions summarized in Table 1. In setting up an experiment first the bottom piston was inserted in the vessel. A Teflon foil sheet (dimensions of 22 mm by 60 mm and thickness of 0.13 mm ± 0.02 mm), was inserted to reduce friction at the vessel wall and to protect the steel from damage by moving quartz grains. The sample material was placed in the vessel using an elongated funnel to prevent grains from sticking to the vessel wall. After putting the sample material in the vessel, the top piston was inserted in the vessel and the vessel was mounted in the Instron loading frame. Before bringing the sample to load, the piston was advanced until touch point (i.e. a small load of 0.05 – 0.06 MPa) by moving it in position control and using the operator-panel control. For experiments at elevated temperature the furnace was switched on to start heating of the sample (before precompaction took place) at a fixed load of 0.0578 MPa. Heating the sample to a temperature of 80°C took about 1 hour. In order to create a locked microstructure, a precompaction phase was applied (Brzesowsky, 1995). To start precompaction the loading frame was switched from position control into load control. Precompaction was done by cycling the applied stress in the range $0.0578\ \text{MPa} \leq \sigma \leq 5\ \text{MPa}$, as indicated in Table 1. After precompaction, the sample was unloaded to touch point load

(~0.0578 MPa), except for the dry experiments. For dry experiments, the sample was loaded immediately after precompaction (so at a load of 5 MPa) to a load of 20 MPa. For wet experiments, after unloading, the fluid flooded test condition was achieved by attaching a vacuum line to the pore fluid in/outlet in the top piston. Upon instantaneous release of the vacuum the pore fluid is flushed into the sample. It is assumed that all of the pore space was filled by the pore fluid when using this method, which was confirmed since samples were extracted wet after termination of the experiment. The experiments were started by advancing the load to 20 MPa. They were left at fixed load for 3-6 days. All loading and unloading ramps during the precompaction and creep experimental stages were performed in 30 seconds.

The experiments were terminated by first unloading the sample by retraction of the piston by 4 mm and removal of the top piston. Subsequently, the bottom piston plus vessel were turned upside down to remove the bottom piston as well. The sample and surrounding Teflon foil was gently pressed out using a steel rod, and it was placed in a cylindrical plastic container. The weight was measured immediately after. The plastic container was kept open to let the sample dry completely. After every experiment with aluminium-chloride, the set-up was cleaned extensively to inhibit any corrosion formation.

2.1.4. Data processing and error analysis

Throughout the experiment force, temperature and position data (both internal Instron position and Sangamo LVDT position) signals were logged at a sampling rate of 1 Hz with a 16-bit NI DAQPad-6015 A/D converter. The Instron resolution was optimized for displacement range expected to occur during the experiment (-10 mm to -20 mm). The Sangamo LVDT was directly calibrated against the Instron LVDT. LVDT position measurements are found to be only linearly dependent on voltage between -5.8 Volt and 5.8 Volt.

Calibration was done using a steel dummy (diameter= 19.35 mm, length= 17.46 mm, material nr: 1.4122), to correct displacement data for apparatus distortion. Calibrations were done both at room temperature and elevated temperatures (T = 80°C). The raw data obtained during the creep experiments was corrected with the sixth order polynomials (fitted through force-displacement data) obtained during the calibration. Prior to data processing the amount of raw data points was reduced, using an excell macro based on a moving average method, to one data point for each 100 data points (i.e. 100 seconds). Sample length, porosity, strain and strain rate were calculated from the averaged and corrected Instron position and external LVDT data.

Analysis of the compaction curves and strain rate data obtained showed that compaction occurring during the initial loading stage plus the following 100 s of all experiments was so rapid it was essentially time-independent. This part of our data was therefore removed from the subsequent (slow) creep stage. Other authors use the same method to cancel out the effect of time-independent creep (Hangx et al., 2010). Finite volumetric strain at any stage was defined as the change in length of the sample with respect to its initial length ($\varepsilon = \Delta L / L_i$).The length of the sample 100 seconds after reaching 20 MPa was used as initial sample length. The starting porosity of each sample was determined using the same initial

length, and they are also displayed in Table 1. Strain rates were calculated using the slope of a line fitted to the strain versus time data. In order to account for the deceleration of creep with time, strain rate was calculated using a variable window size, effectively reducing the amount of strain rate data points. For the first hour after reaching load a strain rate data point was given for every 100 seconds. For the following three hours a strain rate data point was calculated for every 30 minutes. From four hours after reaching load until 20 hours after reaching load a strain rate data point was calculated for every 4 hours. From 20 hours onwards until the end of the experiment, a strain rate data point was calculated for every 10 hours.

2.2. Experimental method – Stress relaxation experiments

The experiments done on sand aggregates were complemented by stress-relaxation experiments on sandstone cylinders, for control purposes. Three experimental conditions were tested: a first with distilled water as pore fluid, a second with aqueous aluminium chloride solution (0.1 M) as pore fluid, and a third with air as pore fluid, i.e. dry (see Table 2). The measured stress decay during the stress-relaxation phase was used to calculate corresponding strain rates (Rutter et al., 1978).

2.2.1. Starting material and sample preparation

Two types of sandstone cylinders were used, Bentheim sandstone (L = 94.45 ± 0.05 mm, diameter = 33.85 ± 0.05 mm, porosity = 24.7%) and Fontainebleau sandstone (L = 73.5 ± 0.5 mm, diameter = 24.7 ± 0.05 mm, porosity = 21.2%). Both were cored perpendicular to bedding and edges were ground parallel. Set-up of the assembly was slightly different for both sample types. For Bentheim sandstone an EPDM sleeve and FEP jacket were fitted around the samples, where the FEP jacket extended to cover the edges of top and bottom piston. Samples were vacuum filled with pore fluid (distilled water or aluminium solution, depending on test condition) in two phases to ensure maximum filling of the pores. The percentage of fluid flooding was determined by the weight difference of a sample before and after fluid flooding and was 95% and 71% for respectively the Bentheim and Fontainebleau samples. To reduce friction between pistons and sample, a Teflon sheet was placed in between. An steel wire tourniquet tightened around the piston and plus jacket at the height of an EPDM band O-ring ensured complete sealing of the sample. Since no piston set was available for 25 mm diameter cores, a silicone tube with an inner diameter of 25 mm and a wall thickness of 5 mm was closely fitted around the samples and two stainless steel spacers. The stainless steel spacers (diameter = 25 mm) were used to extend the cylinders. The length of the silicone tube was such that the spacers were also surrounded by it. The edges of the tube were smooth, to have good closure at both the top and bottom pistons. This alteration enables us to use the 35 mm diameter piston set and subsequent assembly was similar as described above with omission of the EPDM sleeve and second vacuum filling.

The aluminium chloride solution was prepared by dissolution of $AlCl_3 \cdot 6H_2O$ in distilled water and had a concentration of 0.1 M. In the case of the dry experiment, the sandstone cylinder was placed in the oven at 100°C during 1 week, to ensure there was no residual pore water present.

Exp. nr.	Name	Test condition	Precompaction loading	Type of pore fluid	T(˚C)	Duration (days)	Φ_i (%)	pH	Max ε (-)
2	DR2	Dry	1x 30 min, 4x 15 min, 4x 6 min	-	Room T	~ 3	40.04%		1.17E-02
3	DR3	Dry	1x 30 min, 8x 6 min	-	Room T	~ 3	40.02%		1.00E-02
13	DR4	Dry	1x 30 min, 8x 6 min	-	Room T	~ 0.5	40.25%		1.15E-02
16	DR5	Dry	1x 30 min, 8x 6 min	-	Room T	~ 0.5	39.58%		8.83E-03
18	DR6	Dry	1x 30 min, 8x 6 min	-	Room T	~ 0.5	39.71%		1.03E-02
6	HT.DR1	Hot + Dry	1x 30 min, 8x 6 min	-	80ºC	~ 6	39.85%		2.70E-02
5	W2	Wet	1x 30 min, 8x 6 min	distilled water	Room T	~ 6	39.26%	5.5	1.31E-02
12	W3	Wet	1x 30 min, 8x 6 min	distilled water	Room T	~ 3	39.41%	5.5	1.11E-02
7	HT.W1	Hot + Wet	1x 30 min, 8x 6 min	distilled water	80ºC	~ 3	39.76%	5.5	1.89E-02
8	F1.NaSi	Wet /Si	1x 30 min, 8x 6 min	Na2Si3O7	Room T	~ 3	39.18%		1.09E-02
9	F2.AlCl0.1	Wet / AL	1x 30 min, 8x 6 min	AlCl3*6H2O - 0.10 M	Room T	~ 3	39.23%	3.5	7.84E-03
14	F5.ALCl0.1	Wet / AL	1x 30 min, 8x 6 min	AlCl3*6H2O - 0.10 M	Room T	~ 3	38.99%	3.5	8.59E-03
11	F4.AlCl0.01	Wet / AL	1x 30 min, 8x 6 min	AlCl3*6H2O - 0.01 M	Room T	~ 3	38.27%	4.5	8.71E-03
15	F6.ALCl0.01	Wet / AL	1x 30 min, 8x 6 min	AlCl3*6H2O - 0.01 M	Room T	~ 3	39.01%	4.5	9.33E-03
17	F7.NaCl	Wet / NaCl	1x 30 min, 8x 6 min	NaCl - 0.3 M	Room T	~ 3	39.24%	5.5	1.21E-02
19	F8.NaSO4	Wet / Na2SO4	1x 30 min, 8x 6 min	Na2SO4 - 0.15M	Room T	~ 3	39.46%	5.5	1.34E-02
10	HT.F3.AlCl0.1	Hot + Wet	1x 30 min, 8x 6 min	AlCl3*6H2O - 0.10 M	80ºC	~ 5	38.91%	3.5	1.43E-02

Table 1: Overview of compaction experiments performed on sand aggregates. Precompaction cycling of 0.0578 MPa ≤ σa ≤ 5 MPa. All creep experiments performed at load of 20 MPa. φ_i : porosity (%) 100 s after reaching 20 MPa, max ε : volumetric strain (-) reached at end of experiment.

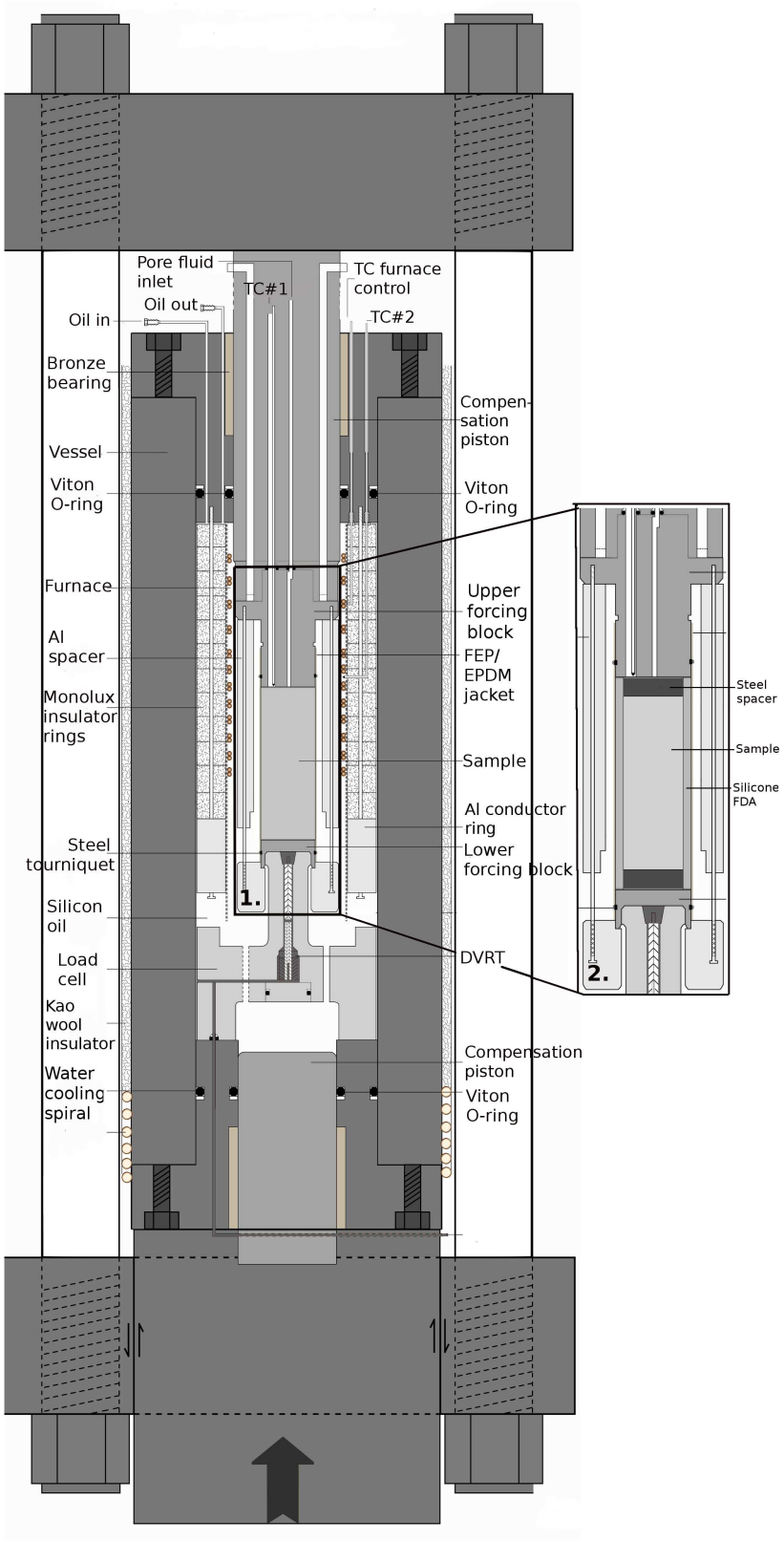

Figure 3: Schematic diagram showing the triaxial deformation apparatus in a yoke assembly. 1: set-up for 35 mm diameter (Bentheim) samples. 2: set-up for 25 mm diameter (Fontainebleau) samples.

2.2.2. Experimental set-up

The experiments were performed using a conventional triaxial deformation apparatus equipped with a pressure balanced yoke assembly. The apparatus thus consists of a self-compensating volume silicon-oil medium pressure vessel (see Figure 3) and an electro-servo-controlled ram for axial loading. The stress relaxation experiments were performed using hard stainless steel (material number: 1.4122) pistons. Confining pressure was applied with a compressed-air diaphragm pump. During the experiment, the confining pressure was regulated using a 20 mL hand pump connected to the pressure vessel. In this way the confining pressure was held constant to be 35 MPa ± 0.1 MPa. The axial load was measured both internally and externally. The external load signal is measured on the electro-servo-controlled ram, and the internal load signal is measured on the loading piston, which is equipped with a Differential Variable Reluctance Transducer (DVRT). This allows us to measure the axial force independent of seal friction between the vessel seals and the loading ram. The load limit was 95 kN. Axial displacement was monitored during the experiments with a Linear Variable Differential Transducer (LVDT) on the electro-servo controlled ram. Temperature was applied using an independently controllable Thermocoax internal furnace with a resolution of 0.1˚C and it was measured using two thermocouples, one located in the top piston and one located in the silicon-oil (see Figure 3). Settings of cooling and location of the aluminium spacer surrounding the sample (see Figure 3) ensured that the temperature gradient along the central axis of the sample is less than 2°C. Experiments were performed at 80°C. Thermal equilibrium was reached 12 hours after switching on the furnace. The pore fluid inlet is left vented to the atmosphere to prevent pore fluid pressure build up.

2.2.3. Testing procedure

Once thermal equilibrium was reached, confining pressure was brought to 35 MPa then the loading ram was advanced until close to touch. The sample was loaded by advancing the ram at 1 μm s^{-1}, which corresponds to a strain rate of 10^{-5} s^{-1}. Once the external load cell registerd 5 kN (i.e. certain touch), the set-up was left to equilibrate. After 1 hour, the load-up was continued at 1 μm s^{-1} displacement rate. The relaxation experiment was started once a load of 85 kN was reached, by holding the loading piston at the current position. The stress relaxation behaviour was monitored for 1 day, without adjusting the temperature or confining pressure.

The experiment was terminated by removing the axial load, switching off the furnace, lowering the confining pressure and leaving the set-up to cool down. After 1 hour the sample was dismantled from the vessel.

2.2.4. Data processing and error analysis

Internal and external load, position, confining pressure, temperature close to the sample and temperature in the silicon-oil were recording with a sampling rate of 1 Hz, as with the compaction experiments, using a 16-bit NI DAQPad-6015 A/D converter. The Instron resolution was optimized for the displacement range expected to occur during the experiment.

Only the first 5 hour block of the monitored relaxation data was processed. Finite volumetric strain at any stage was defined as the change in length of the sample with respect to its initial

length ($\varepsilon = \Delta L / L_i$). The initial sample length was taken to be the length of the sample measured before positioning the sample into the assembly. The stress was calculated using the internal load signal. The internal load signal was corrected for the confining pressure. The data was processed to yield the rate of change of stress ($D\sigma/Dt$) and strain rates ($D\varepsilon/Dt$) during the experiments. Rate of change of stress and strain rate data were calculated by taking the derivatives of respectively the stress versus time and strain versus time data. Note that it is assumed that the measured strain (ε_M) during the experiment is equal to the elastic strain attained during the experiment by the apparatus and the sample (ε_E), plus the permanent strain (ε_P), attained by the sandstone sample. For derivation of strain rate of the sample from experimental data, see Appendix 1.

When deriving final strain rate, only a small number of average data points (10-14 points) was used, in order to reduce noise. The average data points were chosen from the stress decay plot: four points were chosen at a regular interval between t=0 and t=1000 s and from 1000 s onwards, each 1000 seconds one point was chosen at a regular interval until 5000 seconds.

Name	Rock type	Test condition	σ_i (Mpa)	Type of pore fluid and concentration	L_i (mm)	Diameter (mm)	φ_i (%)
SS35.W1	BH	Wet	91.76949321	distilled water	94.4	33.85 ± 0.05	24.70%
SS35.AlCl0.1	BH	Wet	93.12905477	AlCl3*6H2O - 0.10 M	94.5	33.85 ± 0.05	24.70%
SS25.W1	FB	Wet	170.4352121	distilled water	73	24.7 ± 0.05	
SS25.AlCl0.1	FB	Wet	160.822977	AlCl3*6H2O - 0.10 M	72.9	24.7 ± 0.05	21.20%
SS25.D1	FB	Dry	170.784370	-	88.3	24.7 ± 0.05	

Table 2: Overview of stress relaxation experiments performed on sandstone cylinders. All tests were started as soon as the external force signal reached 85 kN. BH: Bentheim sandstone, FB: Fontainebleau sandstone, σ_i: starting stress (MPa), L_i: length of sample before loading (mm), φ_i: initial porosity (%).

3.1. Results of uniaxial compaction creep experiments

To illustrate the effect of chemical environment on the creep of quartz sand aggregates, compaction creep curves (ε vs. t) and log-log plots of volumetric strain rate ($\dot{\varepsilon}$) versus volumetric creep strain (ε) are shown in Figure 4-9. All data were obtained from creep tests performed on material with a similar initial grainsize, at an applied axial stress of 20 MPa. As discussed above, the strain displayed in the log-log plots does not includes ramping strain and strain produced during pre-compaction, since it is assumed all to be time independent compaction creep.

3.1.1. Dry experiments

The experiments done on dry sand aggregates show a wide distribution in compaction curves. Figure 4 shows all dry experiment compaction curves plus the results of the two fluid flooded experiments with distilled water as pore fluid. In Figure 5 the corresponding log strain rate versus log strain curves are given. The large spread seen in both figures indicates

bad reproducibility for the dry experiments. No comparison on compaction creep can be made between the dry and water flooded experiments.

3.1.2. Wet experiments

Two experiments with distilled water as pore fluid were performed. The resulting compaction curves and log-log plots of volumetric strain rate versus strain are shown in figure 6 and 7. Experiment W2 shows slightly more compaction and higher strain rates at constant strain, than experiment W3. The water-flooded experiments are in good agreement, which indicates good reproducibility.

The compaction curves and log-log plots of volumetric strain rate versus strain for the experiments with aluminium chloride, sodium silicate, sodium chloride and sodium sulfate solution as pore fluid are also plotted in Figure 6 and 7. All aluminium chloride solution experiments (F2.AlCl0.1, F5.AlCl0.1, F4.AlCl0.01 and F6.AlCl0.01) and the sodium silicate solution experiment (F1.NaSi) show less compaction and lower strain rates at constant strain than the water flooded experiments. The 0.01 M aluminium chloride solution experiments (F4.AlCl0.01 and F6.AlCl0.01) show more compaction and larger strain rates at constant strain than the 0.1 M aluminium chloride solution experiments (F2.AlCl0.1 and F5.AlCl0.1). Aluminium chloride flooded experiments have good reproducibility, similar to the reproducibility of the water-flooded experiments. The sodium silicate experiment shows more compaction and larger strain rates at constant strain than all aluminium experiments, but less than the pure water experiments. Sodium sulfate (F8.NaSO4) and sodium chloride solution (F7.NaCl) experiments show more compaction and larger strain rates at constant strain than the water flooded experiments. Sodium sulfate solution shows even more compaction and larger strain rates at constant strain than the sodium chloride solution.

In short, different pore fluids cause differences in the compaction creep. Considering water flooded experiments (W2 and W3) as reference, compaction creep is inhibited by aluminium chloride (experiments F2.AlCl0.1, F5.AlCl0.1, F4.AlCl0.01 and F6.AlCl0.01) and by silica saturated solution (experiment F1.NaSi). The inhibiting effect of silica saturated solution (experiment F1.NaSi) is smaller than the effect of both aluminium chloride solutions. Compaction creep is enhanced with sodium chloride or sodium sulfate (experiments F7.NaCl and F8.NaSO4) as pore fluid.

3.1.3. Effect of temperature on compaction creep

Three experiments were done at a temperature of 80°C. One dry experiment, one experiment with distilled water and one experiment with 0.1 M aluminium chloride solution. The corresponding compaction curves and the log-log plot showing the dependence of volumetric strain rate on volumetric creep strain are shown in Figure 8 & 9. For comparison the results for the same experiments but then at room temperature (DR2, W2, F2.AlCl0.1 and F5.AlCl0.1) were plotted as well. Data of dry experiment DR2 was chosen since it represents an average value of the dry experiments. Overall, all experiments at 80°C result in higher strains and larger strain rates at constant strain, when compared to experiments conducted at room temperature.

The difference in trend between the dry experiment (HT.DR1) and experiment with water added as pore fluid (HT.W1) for the high temperature experiments can be clearly observed

in Figures 8 & 9. For the first 18 hours the strain and strain rates at constant strain in the wet experiment are higher when compared to the dry experiment. From ~18 hours onwards, strain and strain rates at constant strain in the dry experiment are larger than in the experiment with water as pore fluid. The dry and water flooded experiment at room temperature are similar to each other.

In Figure 8 & 9, the difference in aluminium chloride and water flooded experiments performed at elevated temperature can be observed. At high temperature the aluminium chloride flooded experiment (HT.F3.AlCl0.1) shows less compaction and lower strain rates at constant strain when compared to the water flooded experiment (HT.W1). This effect of aluminium chloride was also observed for experiments on room temperature.

Qualitatively the effect of chemical environment was the same for both low and high temperatures: addition of 0.1 M aluminium chloride solution resulted in inhibited compaction creep. However, the amount of creep reduction by adding aluminium chloride is larger for the experiments at elevated temperature than for room temperature. The offset between the dry and water flooded experiments at 80˚C is not observed with the room temperature experiments.

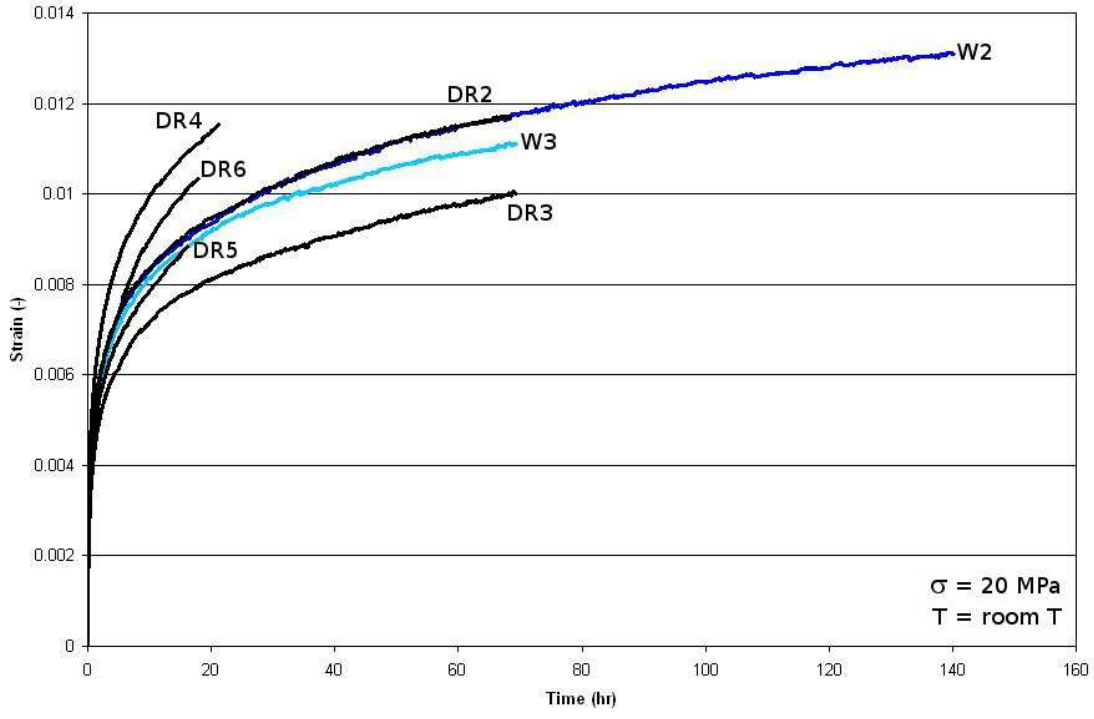

Figure 4: Compaction creep curves of dry (black lines) and water flooded (blue lines) experiments.

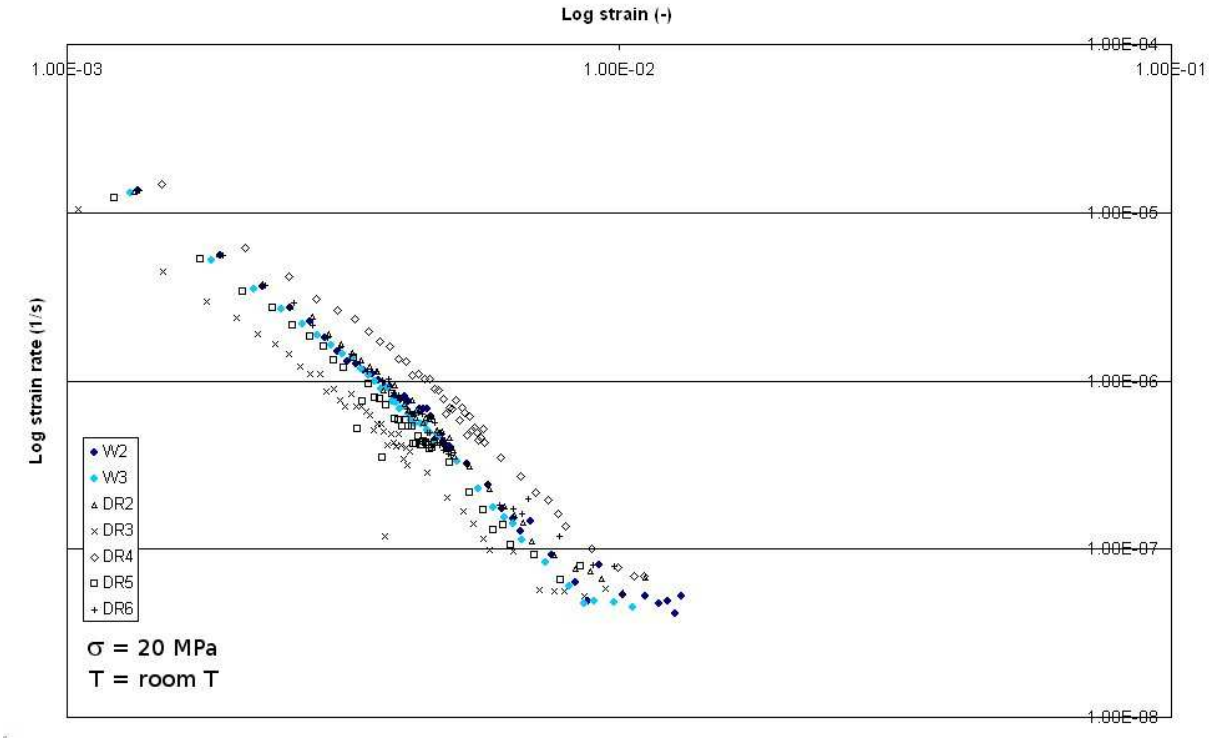

Figure 5: Log-log plot of volumetric strain rate ($\dot{\varepsilon}$) versus volumetric creep strain (ε) for dry (black symbols) and water flooded (blue dots) experiments.

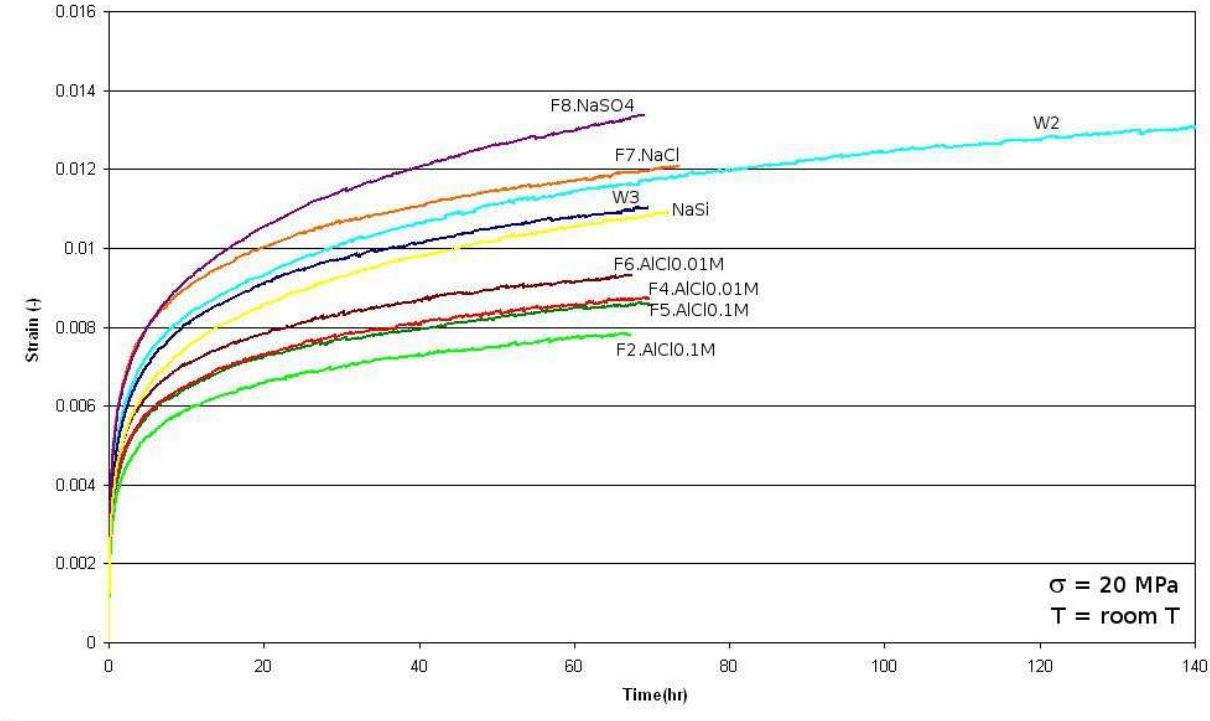

Figure 6: Compaction creep curves of all fluid flooded experiments.

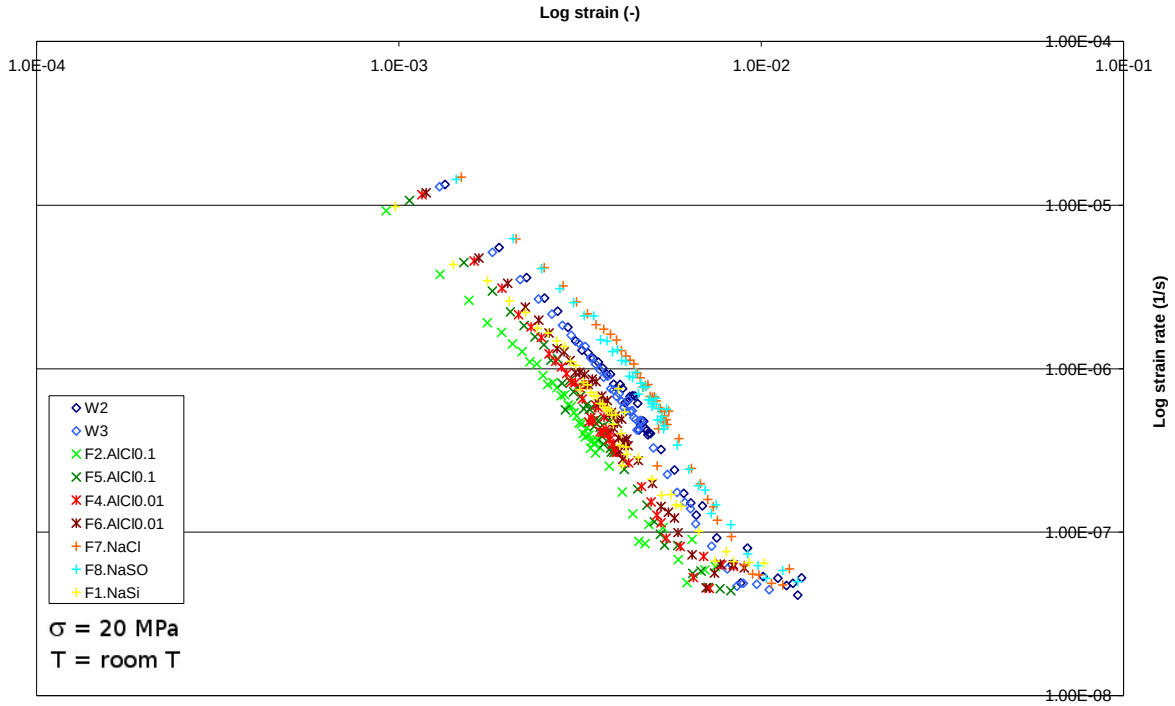

Figure 7: Log-log plot of volumetric strain rate ($\dot{\varepsilon}$) versus volumetric creep strain (ε) for all fluid flooded experiments.

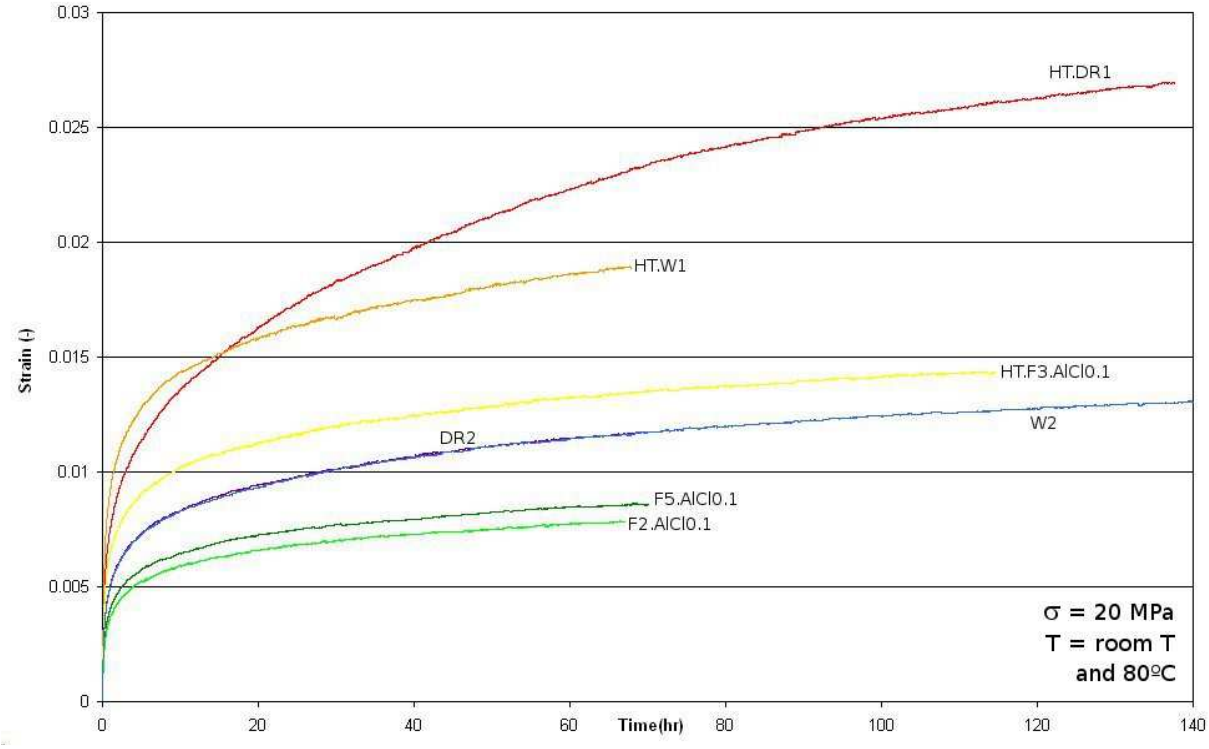

Figure 8: Compaction creep curves of high temperature and corresponding room temperature experiments.

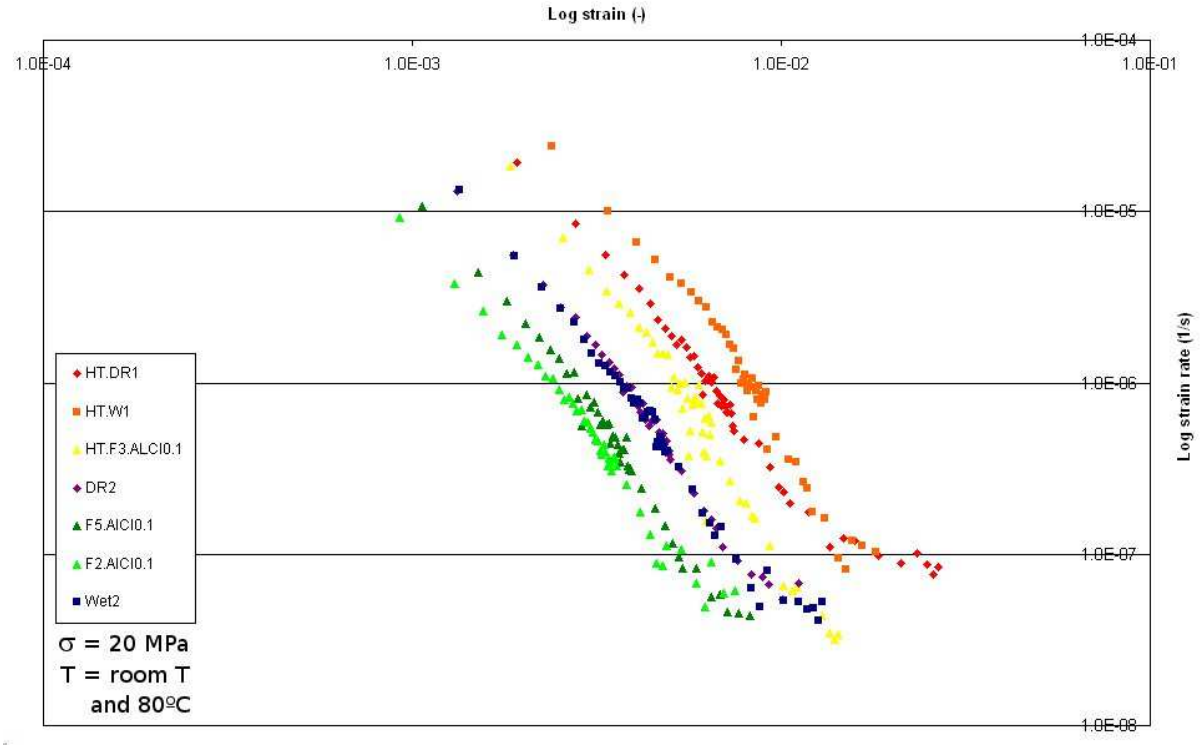

Figure 9: Log-log plot of volumetric strain rate ($\dot{\varepsilon}$) versus volumetric creep strain (ε) for high temperature and corresponding room temperature experiments.

3.2 Results of stress relaxation experiments

The experiments were performed by loading the sandstone cores to a load of 85 kN at a strain rate of 10^{-5} s^{-1}. At a load of 85 kN the position was kept constant and stress decay as a function of time was measured. There are small offsets in the stress reached at maximum load caused by the minor difference in confining pressure between the performed experiments. Therefore two different y-axes were used to plot two experiments at the same time and the scale was chosen such that the stress at the start of the relaxation period of the two experiments plotted in the same location (see Figure 10, 12 and 13). Doing so enables us to compare the stress decay over time of two experiments (e.g. water and aluminium chloride flooded). Note that the offset is also reflected in the log-log plots (see Figure 11 and 14).

3.2.1. Bentheim samples (diameter=35mm)

The stress relaxation experiments performed on Bentheim sandstone cores resulted in the stress versus time curve shown in Figure 10 and the log-log plot showing strain rate versus stress shown in Figure 11.

During the first 30 minutes of the stress relaxation experiment both the core with distilled water as the one with 0.1 M aluminium chloride solution follow the same trend, where the stress drop is similar (1.1 ± 0.1 MPa) for both experiments. After 30 minutes the stress for the aluminium chloride solution experiment remains constant, where the distilled water experiment still shows a continuously decelerating change in stress until about 1 hour after the start of the experiment, at which point the stress decays linear with time. In Figure 11 the dependence of strain rate on stress is displayed, on a log-log plot. The difference between

water as pore fluid or aluminium chloride solution can clearly be observed. Figure 11 shows similar trends to Figure 10. Compaction creep is clearly inhibited by the presence of aluminium chloride solution after the first 30 minutes (Figure 10 and 11).

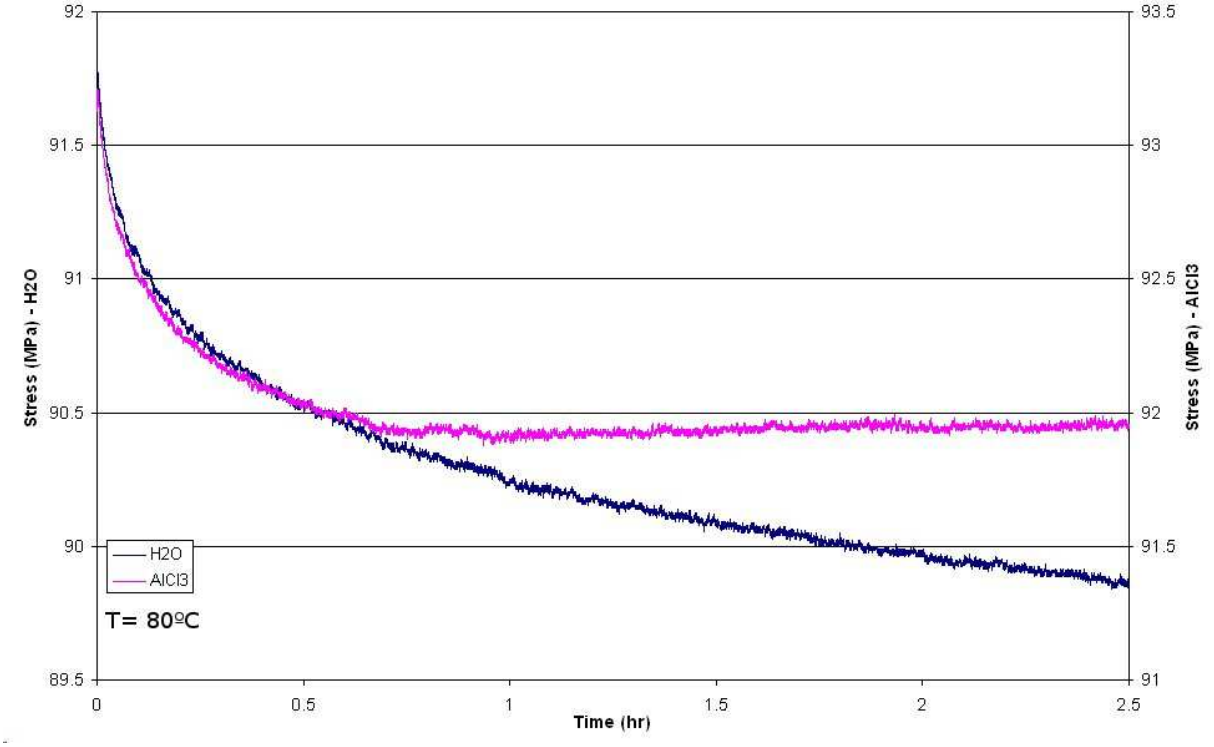

Figure 10: Stress versus time curve for the, 35 mm diameter cylinder, water and aluminium chloride flooded experiments. Note that the two curves are plotted on different y-axes.

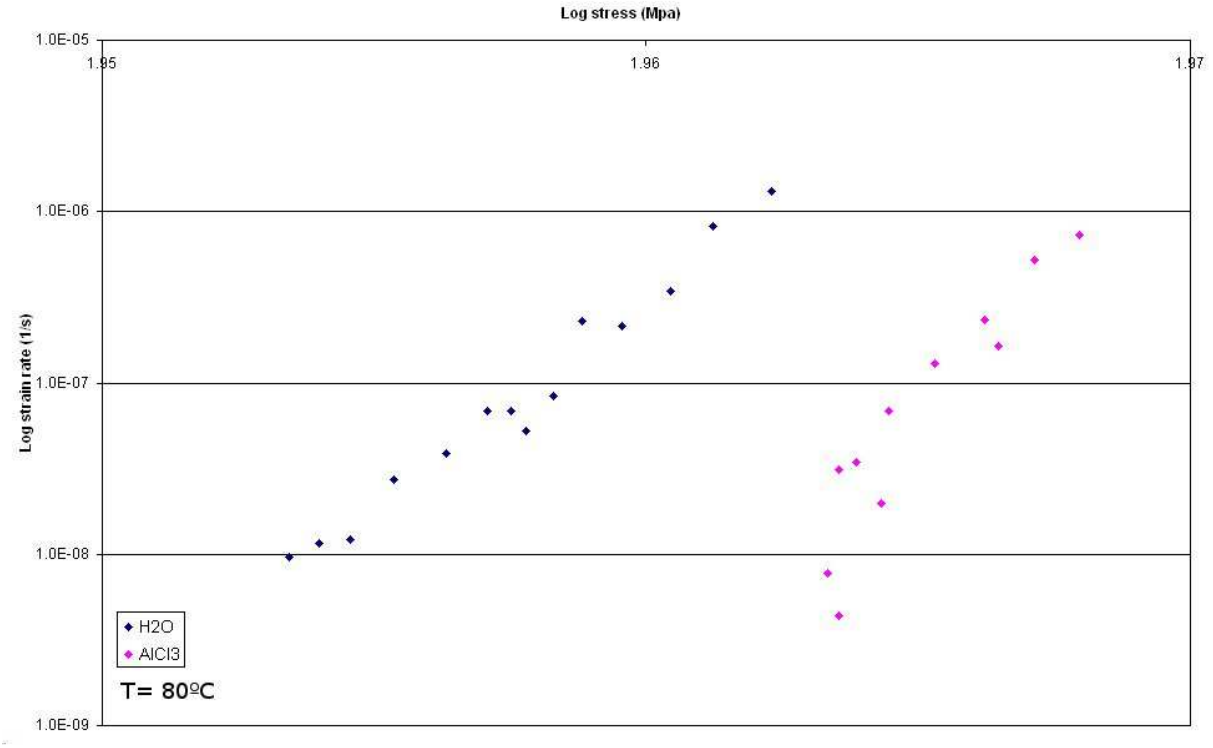

Figure 11: Log-log plot of volumetric strain rate ($\dot{\varepsilon}$) versus stress for water and aluminium chloride flooded experiments.

3.2.2. Fontainebleau samples (diameter=25mm)

Stress relaxation experiments performed on Fontainebleau sandstone cores resulted in the curves shown in Figure 12 & 13. In Figure 12 the stress versus time curves of the water and aluminium chloride experiments are plotted. In Figure 13 the water experiment is again plotted, but now together with the dry experiment. Figure 14 shows the log-log plot of strain rate versus stress results. Note again the offset in starting stress.

All experiments show a continuously decelerating change in stress (Figure 12 and 13). The total stress relaxation after 1.5 hour in both the aluminium flooded experiment (2.68 MPa) and in the dry experiment (3.03 MPa) is larger than the stress relaxation in the water flooded experiment (2.51 MPa). For the water flooded experiment there is a small increase in stress, after approximately 1 hour and 40 minutes. After 20 minutes of stress inversion, stress relaxation continuously decelerates similar as before (see Figure 12). No such stress changes were observed for the other two experiments. For the aluminium chloride and water flooded experiments strain rate decelerates continuously with decreasing stress (Figure 14). The dry experiment shows different results, because the starting strain rate is slower than for the other two. The trend is similar, strain rate developing linear with stress, with a similar slope as the other two experiments (see Figure 14). Based on the results presented in figure 12, 13 and 14 it can be concluded that compaction creep for the dry and aluminium chloride flooded experiments is larger than for the water flooded experiment.

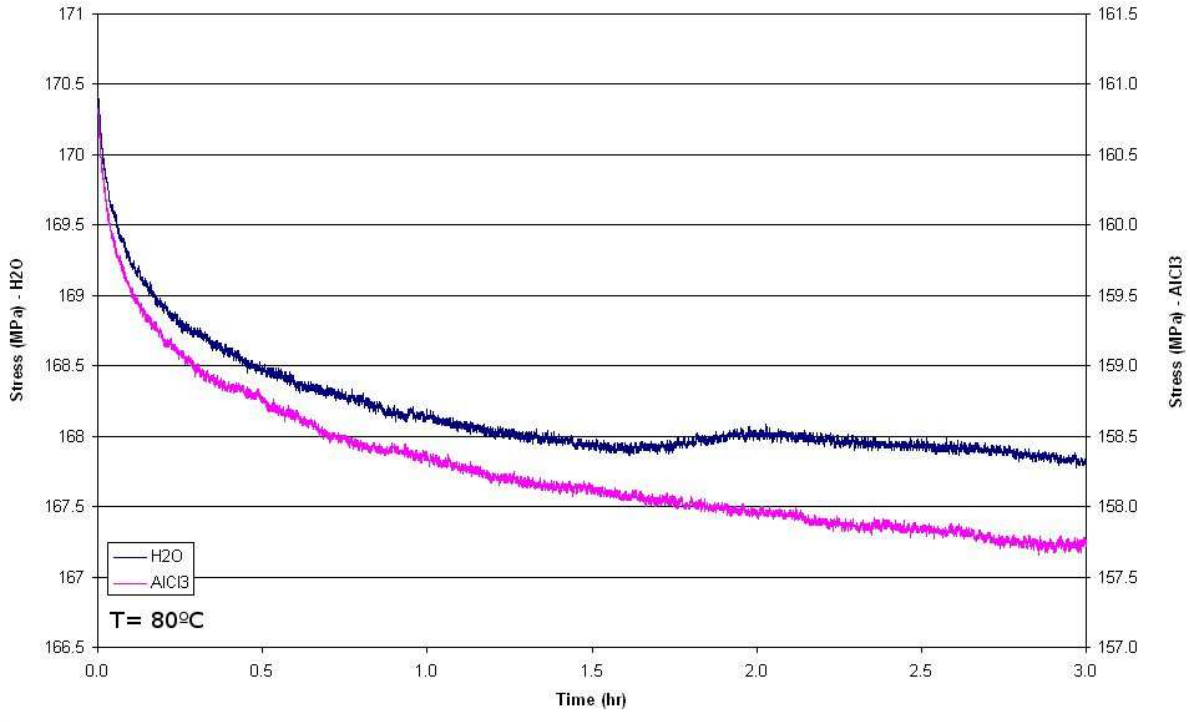

Figure 12: Stress versus time curve for Fontainebleau sandstone. Water and aluminium chloride flooded experiments. Note that the two curves are plotted on different y-axes.

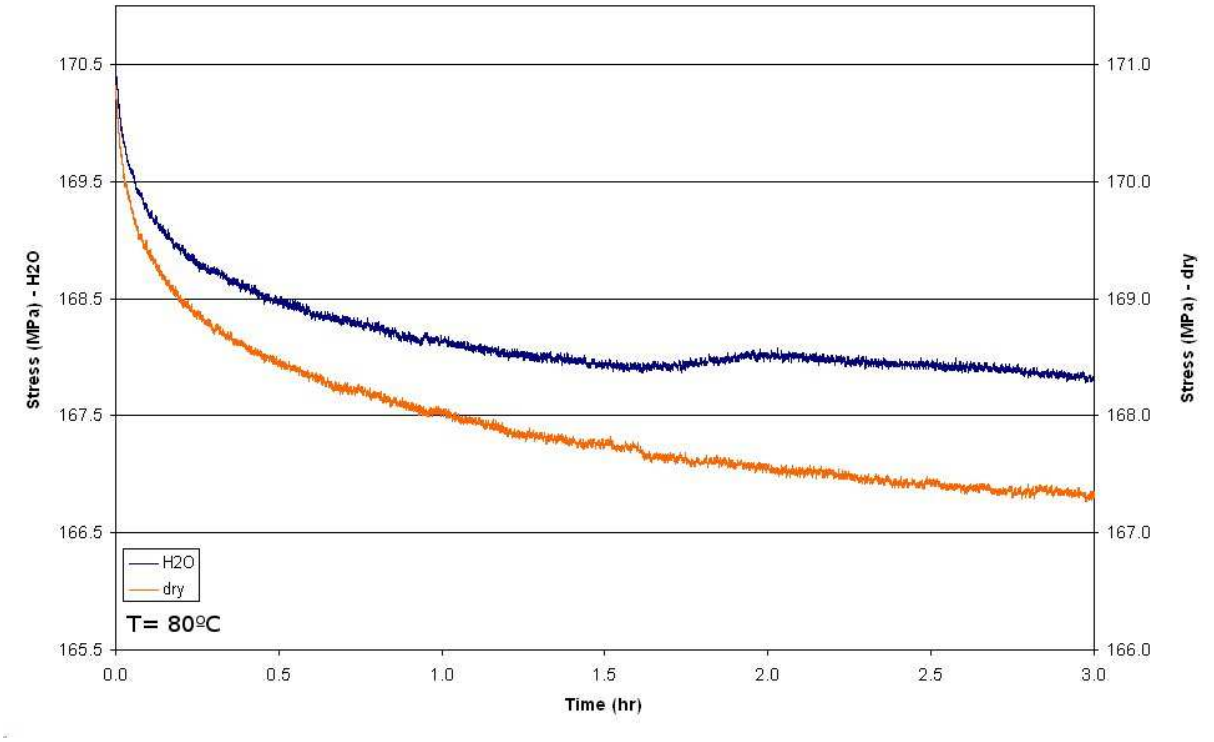

Figure 13: Stress versus time curve for Fontainebleau sandstone. Water flooded and dry experiments. Note that the two curves are plotted on different y-axes.

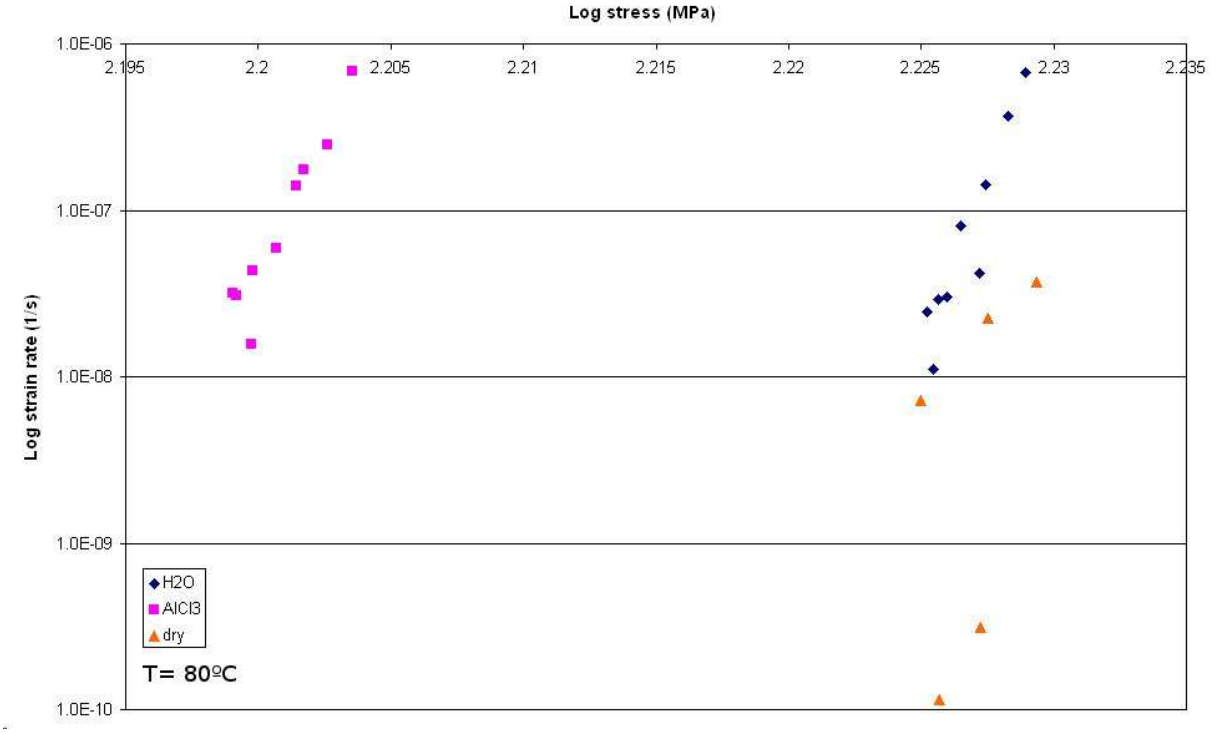

Figure 14: Log-log plot of volumetric strain rate ($\dot{\varepsilon}$) versus stress for water, aluminium chloride flooded and dry experiments.

4.1. Discussion of uniaxial compaction creep experiments

Uniaxial compaction creep experiments are performed both at room temperature and at 80°C on Beaujean sand aggregates aiming to find a suitable additive which will inhibit compaction creep. Comparing the dry and water flooded experiments performed at room temperature, no enhanced effect of water was observed, attributed to the bad reproducibly of the dry experiments. Other studies did observe enhanced compaction creep with availability of water (Chester et al., 2005; Brzesowsky, 1995; Hangx et al., 2010), so we will assume water has an enhanced effect. Comparing water flooded experiments performed at room temperature we found aluminium chloride and sodium silicate as pore fluid causes inhibited compaction creep, whereas sodium chloride and sodium sulfate as pore fluid cause enhanced compaction creep. The experiments performed at 80°C also show the inhibiting effect of aluminium solution. However, the inhibiting effect is larger for the experiments at elevated temperature than for room temperature experiments.

4.1.1. Deformation mechanism

Theoretically, mechanisms for compaction creep in wet granular quartz tests, with or without additives, include: 1) dissolution at grain contacts due to undersaturation of the pore fluid with respect to the solid, 2) pressure solution at grain contacts, 3) subcritical crack growth at grain contacts, 4) subcritical grainscale microfracturing, and 5) grain rearrangements. Subcritical crack growth is defined as: the extension of pre-existing cracks occurring at stress intensity factors lower than the critical stress intensity factor (Atkinson, 1987). Prior to our experiments, the sand aggregates were precompacted to create a locked aggregate. After locking of an aggregate by grain rearrangement further compaction can only be achieved by deformation of the grains and grain contacts. Brzesowsky (1995) performed uniaxial compaction creep experiments on sand aggregates similar to the experiments performed in this study. To test the locking effect of precompaction, Brzesowsky (1995) flooded dry samples with n-decane. It turned out that frictional compaction processes (particle sliding with no chemical effect) played a minor role during the creep tests with n-decane. Hangx et al. (2010) also did similar experiments on sand aggregates to the experiments performed in this study. Hangx et al. found that strain rates were too slow for pressure solution or dissolution processes to be the creep controlling process in quartz. Hangx et al. observed microstructural evidence for grain scale cracking and creep dependence on the type of pore fluid (i.e. chemical properties of the pore fluid). Therefore, the authors concluded that grain scale failure by subcritical crack growth and grain rearrangement are the main mechanisms for creep in quartz. Hangx et al. did not perform any load cycling (e.g. precompaction phase) prior to the experiments, which might explain the contribution of grain rearrangements on compaction creep.

Because of similarity of our experiments with the experiments performed by Hangx et al. (2010) and Brzesowsky (1995), it is assumed that the main process during time dependent creep, in our experiments, was grain scale failure involving subcritical crack growth (i.e. microcracking). When looking closer at the mechanisms of subcritical crack growth; without any chemical agents present cracks can grow by lateral motion of atomic kinks along the crack front during thermal activation, with fluids present a specific type of subcritical crack growth called stress corrosion cracking is active. During stress corrosion cracking strained Si-O bonds at crack tips react more readily with an environmental agent (i.e. water or any other solution) than unstrained bonds. This occurs because of strain induced reduction in the

overlap of atomic orbitals (Michalse and Freiman, 1982, in Atkinson, 1987). The strained bonds can be broken at lower stresses than the unweakened bonds. Factors controlling subcritical crack growth are temperature, the components defining chemical equilibrium, rock microstructure and the effective stress (Atkinson, 1987).

In our room temperature experiments the only variable was the chemical component, which could influence chemical equilibrium. The effect of the temperature factor was tested because experiments were repeated on 80°C. From our results it can be concluded that with aluminium chloride and sodium silicate solutions as pore fluid the rate of creep presumably by microcracking, is decreased, while with sodium chloride and sodium sulfate the rate of creep presumably by microcracking, is increased, for a quartz sample. This is probably due to different interactions of the solutions tested with the strained Si-O bonds at crack tips. Furthermore, creep presumably by microcracking is enhanced with increasing temperature, probably because thermal activation increases the rate of subcritical microcracking (Atkinson, 1984). In the following sections we will try to find an explanation for the enhancing and inhibiting effects on microcracking of the solutions and temperatures tested. We will first discuss the effect of pH, go on to discuss the effect of impurities, salts and silica saturated solution on the dissolution and solubility of quartz, and discuss the effect of temperature. Finally, we will show that the observed results of the different solutions fit with the theories discussed before.

4.1.2. Effect of pH

The pore fluid solutions tested have different pH values, see Table 1. Possibly, the pH effect can explain the dependence of compaction creep on type of pore fluid. Stress corrosion cracking in quartz is pH dependent (Dove, 1995).

At low pH ($pH \approx pH_{PZC}$), the interaction of strained Si-O bonds with water at the crack tips produces weaker, hydrogen-bonded, silanol groups via the following hydrolysis reaction:

(1) $\equiv Si - O - Si \equiv + H_2O \leftrightarrow \equiv Si - OH \bullet HO - Si \equiv$

The silanol surface groups ($Si - OH$) are only weakly joined by hydrogen bonds ($\bullet$), while the siloxane groups ($\equiv Si - O - Si \equiv$) are stronger joined by silicon-oxygen bridging bonds. Because of this, the silanol groups (i.e. weak bonds) are more prone to rupture than the siloxane groups (i.e. strong bonds), leading to enhanced crack growth.

With increasing pH ($pH > pH_{PZC}$), the quartz surface becomes negatively charged, because of formation of $\equiv Si - O^-$ surface groups via the following reaction:

(2) $\equiv Si - O - Si \equiv + OH^- \leftrightarrow \equiv Si - O^- + \equiv Si - OH$

Due to the negative charge of the quartz surface water molecules will be electrostatically reorientated, which will increase interaction of protons with the quartz surface. With increasing pH the relative contribution of water (i.e. reaction 1) and OH^- dominated mechanisms (i.e. reaction 2) to the net fracture rate are changing. Reaction 1 will result in less aggressive attack (i.e. corrosion) of the silica compared to reaction 2. Therefore the relative contribution of reaction 2 increases faster with increasing pH, compared to the contribution of reaction 1. This leads to an increase in crack growth rate with increasing pH, dominated by OH^- attack of the silica surface. The resulting quartz fracture rate dependence on pH is illustrated by Figure 15. Rate of fracture is lowest in acidic solutions having a pH near 2.

Rates increase with increasing solution pH until reactivity begins to level off in alkaline solutions with a pH > 11 (Dove, 1995).

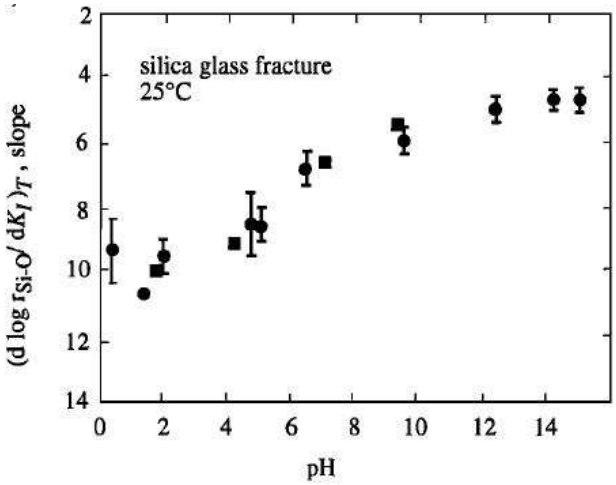

Figure 15: Silica glass fracture rate dependence on pH (Dove, 1995).

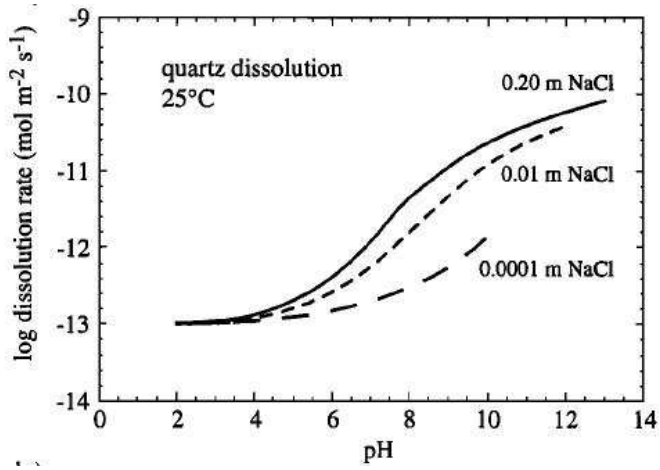

Figure 16: Dissolution rate dependence on pH. Rates increase with ionization of both surface and solvent, which promotes a transition to a reaction mechanisms involving OH^- (Dove, 1994).

The pH of distilled water, 0.01 M aluminium chloride and 0.1 M aluminium chloride solution solution are respectively 5.5, 4.5 and 3.5. According to the pH dependence of fracturing in quartz, 0.1 M or 0.01 M aluminium chloride as pore fluid results in reduced fracture rates, when compared to the fracture rate during water flooded experiments. This observation fits with the earlier described results, where compaction creep is inhibited with aluminium chloride present as pore fluid. However, sodium chloride and sodium sulfate solutions also have a pH of 5.5, so the acceleration of creep rate can not be caused by the difference in pH. So the effect of pH can only partially explain our results.

4.1.3. Effect of impurities on quartz dissolution and fracturing

The presence of aluminium, sodium and chloride impurities influence microcracking because such impurities also affect dissolution and solubility of quartz, and quartz fracturing and dissolution processes can be considered similar. Subcritical fracture approximates dissolution through the relative slow rupture of chemical bonds at rates that are not limited by the flow of fluid from the material in the fracture void space (Renshaw and Pollard, 1994).

This leads to the suggestion that processes governing subcritical fracture and dissolution likely proceed by similar pathways. Thus, theories of chemical controls on mineral dissolution may also describe the effect of chemical environment on subcritical fracture rates (Dove, 1994). The similarity of silica fracture and dissolution rates is illustrated by the similar pH dependence (Figure 15 & 16). The effects of aluminium, sodium and chloride ions on quartz solubility are therefore investigated.

Jephscott and Johnston (1950) were one of the first to research the effect of aluminium on the solubility of silica. They have shown that the apparent solubility of amorphous finely divided silica in water, which they find to be 0.017% at 37˚C, is reduced to 0.003-0.0097% when aqueous aluminium oxide is added to the system and to less than 0.0001% when powdered aluminium is present. Iler (1973) has shown that aluminium impurities reduce not only the solubility of silica at equilibrium by chemisorption on the surface of silica, even in amounts less than a monomolecular layer, but also the rate of dissolution of silica (see Figure 17) (Iler, 1973). The amount of aluminium on the silica surface required to reduce the solubility of silica has been measured by Iler (1973). When only one aluminium atom was absorbed on the surface as an anionic aluminiumsilicate per 2 nm^2, at which point only 5% of the surface was occupied, the rate of dissolution as well as the equilibrium solubility of the surface were drastically reduced. At high aluminium concentrations, the rate of dissolution drops to zero after very little silica has been dissolved, suggesting that the equilibrium solubility of the surface is very low, even though the amount of aluminium is less than the amount required to cover the silica surface (Iler, 1973). Note that the experiments performed by Iler (1973) are performed in solutions with high pH, which will lead to a maximum effect. Comparing this to our experiments the aluminium solutions have low pH (3.5 for the 0.1 M and 4.5 for the 0.01 M solution), so quantitatively, the study of Iler can not be compared with our study. Qualitatively, however, the study of Iler and our study can be compared.

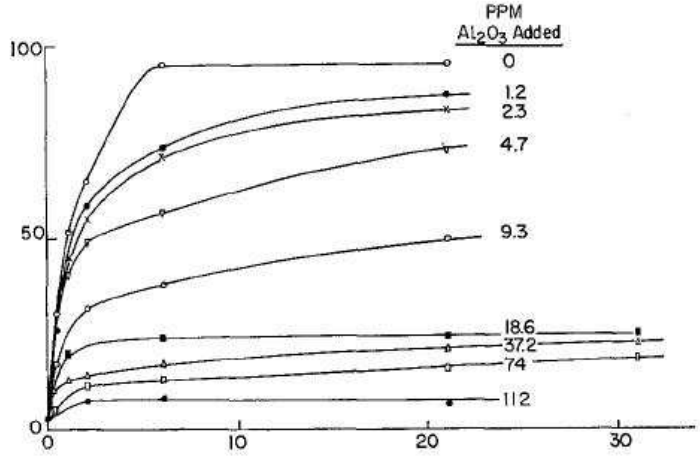

Figure 17: Dissolved SiO_2 (ppm) versus time in days, at 25˚C. Increasing concentration of silica with time, as silica dissolves from colloidal particles into an initially undersaturated solution in water in the presence of different concentrations of aluminium in system (Iler, 1973).

In the present study, experiments were performed with sodium chloride (i.e salt in solution) as pore fluid. Compaction creep was enhanced by sodium chloride solution. The effect of salts on the solubility and microcracking of quartz is therefore important to discuss. Several studies on the effect of salts on silica dissolution found that the presence of salts enhances

silica solubility plus rate of dissolution (Iler, 1979 and references therein). Dienert and Wandenbulcke (1923) reported that colloidal silica passed into solution as soluble silica and that alkalinity and salts were good catalysts for dissolution. Van Lier (1965) found that sodium chloride increased the rate of solution of quartz in water by factors of respectively 4, 14 and 67 in 10^{-3}, 10^{-2} and 10^{-1} N solutions. The enhanced solubility of quartz by sodium impurities occurs because sodium ions weaken and attack Si-O bonds in quartz surfaces by the formation of $\equiv Si-O^{-}Na^{+}$ ion pair surface complexes (Wirth and Gieskes, 1979; Dove, 1994). The bond angle is increased for the $\equiv Si-O^{-}Na^{+}$ surface complexes while the Si-O bond angle is stretched in comparison to the Si-OH surface complexes (Lasaga and Gibbs, 1990). Because of this, the $\equiv Si-O^{-}Na^{+}$ surface complex (i.e. Na^{+} weakened bond) is more prone to rupture than the Si-OH surface complexe (i.e. non-Na^{+}-weakened-bond), leading to enhanced dissolution and microfracturing of quartz at the $\equiv Si-O^{-}Na^{+}$ surface complexes. Additionally, Na^{+} ions in the surface complex enhance local dissociation of water, providing OH^{-} ions for attack of Si atoms (as discussed earlier in section 4.1.2.) and leading to the rupture of Si-O bonds (see Figure 16) (Dove, 1995).

4.1.4. Effect of saturated silica solution

The results of the sodium silicate solution experiment show only a minor amount of compaction creep reduction, compared to the water flooded experiments, despite the fact that the solution was silica saturated. However, since the presence of sodium ions increases the rate of microcracking and since the silica saturation level slows down the rate of microcracking, it can be inferred that both additions have competing effects. The effect of silica saturation thus appears to be slightly more effective.

4.1.5. Effect of temperature

Based on our experiments it can be stated that with increasing temperature conditions microcracking enhances. Furthermore, aluminium chloride solution also inhibits compaction creep at 80°C, although the quantitative inhibiting effect is larger at 80°C than at room temperature. The observed results are consistent with the general ideas of thermal activation. Thermal activation speeds up dissolution and fracturing by lowering the activation energy (Atkinson, 1979).

4.2. Discussion of stress relaxation experiments

Two sets of stress relaxation experiments are performed, one set on Bentheim (diameter=35mm), and one set on Fontainebleau (diameter=25mm) sandstone cylinders. The results of the Bentheim cylinders are consistent with the results of the sand aggregate experiments: the presence of aluminium chloride inhibits compaction creep compared to water flooded experiments. We assume that the Bentheim sandstone cylinders deform by the same mechanism (i.e. micro cracking) as the sand aggregates, following the reasoning described in section 4.1.1. The previous discussion about the factors controlling the rate of stress corrosion: pH of the pore fluid and effect of impurities also applies to the Bentheim sandstone experiments. The observed creep reduction is either the result of the lower pH of the aluminium chloride solution, or the result of aluminium ions slowing down the quartz dissolution process by chemisorption on the silica surface, or a combination. We assume that aluminium has a similar effect on stress corrosion cracking of the Bentheim samples as for the compaction creep experiments. The Fontainebleau sandstone cylinder experimental

results do not show any inhibiting effect of aluminium chloride. In stead, the results implicate that creep is enhanced for the aluminium chloride solution and dry condition, when compared to the water flooded experiment, which conflicts with general concepts of microcracking. This is probably related to the fact that the results illustrate processes other than creep and can be caused by the different piston set-up of the experiment or by the material properties. First we will try to fit the Bentheim results to a microphysical model, and then we will try to find an explanation for the Fontainebleau results by discussing the set-up and material properties.

4.2.1 Betheim experiments

In the Bentheim cylinder experiments stress development for the first 30 minutes is similar for the water and aluminium chloride flooded experiments. After 30 minutes creep is clearly inhibited by the presence of aluminium chloride solution (Figure 10 and 11). In order to explain this delayed effect we have to think about initial structure and we developed a qualitative microphysical model. In each sample an initial amount of micro cracks will be present (i.e. flaws). The largest and best orientated flaws will fail first during compaction. For smaller flaws to fail the crack length needs to be increased by stress corrosion cracking. During the first 30 minutes of the stress relaxation experiment the largest flaws fail. From 30 minutes onwards all the large flaws failed and smaller flaws need to be lengthened: stress corrosion cracking needs to occur before the sample can compact and stress can be released. In the aluminium chloride experiment stress corrosion cracking is inhibited, while in the water experiment stress corrosion cracking is still active and can cause compaction creep. This causes the offset in Figure 10. Another possibility is that the presence of aluminium chloride inhibits creep for the complete relaxation experiment. In this case, the aluminium chloride experiment would show a stress drop that is continuously less decelerating than the stress drop in the water flooded experiment. This does not fit with our observations. Also, the strain rates measured for the aluminium experiment should be lower than the strain rates of the water flooded experiment.

4.2.2. Fontainebleau experiments

The results of the Fontainebleau experiments show that creep in the dry and aluminium chloride solution experiments is larger than in the water flooded experiment (Figure 12 and 13). Water flooded experiments should show more creep than dry experiments according to the general concepts of stress corrosion cracking (Rutter et al., 1978; Atkinson, 1987). The results are also not consistent with the uniaxial compaction creep experiments and Bentheim sandstone stress relaxation experiments. The Fontainebleau cylinder experiments were expected to give better results than the Bentheim cylinder experiments, because a stress closer to the failure stress could be reached due to the smaller sample dimensions. Performing the stress relaxation test close to the failure stress would result in the highest strain and strain rates. The exact failure stress was estimated in advance by performing a failure test on both a wet 25 mm and 35 mm diameter sandstone sample. Both tests were unsuccessful, because no failure would occur before the upper force limit of the apparatus was reached. For the 35 mm diameter samples a force of 85 kN corresponds to an applied stress of 45.5 ± 0.5% of the failure stress (Klein et al., 2000). For the 25 mm diameter samples a force of 85 kN corresponds to an applied stress of 72.3 ± 2.5% of the failure stress (Sulem et al., 2006). The strain rates observed for Fontainebleau sandstones are similar to the strain rates observed in Bentheim experiments, which is striking because the stress reached in

Fontainebleau experiments is higher. For all the experiments the strain rate was calculated and plotted in a similar way. Processes other than grain cracking and failure might cause the observed stress relaxation trend in Fontainebleau sandstone. Possibilities are differences in experimental set-up or differences in material properties between the used Fontainebleau samples.

The Fontainebleau experiments have a different piston set-up than the Bentheim experiments, which could explain the different results. Another factor which might be of importance is the confining pressure drop during the experiments. During the Fontainebleau experiments 25 mm diameter samples were surrounded by a silicon tube and compacted using the 35 mm piston set. If the silicon tube was squeezed between the piston and the sample this might affect the stress relaxation behavior. The silicon tube tightly fitted around the sample and was deformable enough not to affect the measured compaction creep. After the experiment no indicators were found that the silicon tube material was squeezed between the sample and the pistons, ruling out the effect the tube might have on the observed results. During all stress relaxation experiments confining pressure dropped by 0.5 ± 0.2 MPa over one day, by leaking onto the sample via the top piston (i.e. no complete sealing). Because the pressure drop occurred in all experiments this feature can also not explain the Fontainebleau results. The effect of the silicone oil present in the sample will be minimal, because the oil is chemically inert. The measured internal stress is corrected for the confining pressure, so the effect of a leak is not observable in our data.

The material properties of the Fontainebleau sandstone could also explain the observed results. Factors that are considered are: the presence of carbonate cement, Fontainebleau sample heterogeneity and deformation mechanisms. Carbonate cement can react with the pore fluid and the reaction product can affect the strength of the sample. To test the presence of carbonate cement in the Fontainebleau sandstones, a small amount of respectively 0.1 M aluminium chloride and hydrochloric acid (10% solution) was dropped on the sample. If carbonate is present it will react with the mentioned solutions, which can be observed. However, no carbonate was found present in the sandstone, effectively ruling out the presence of carbonate cement as a cause of the observed Fontainebleau results. Heterogeneity of the Fontainebleau samples can also explain the results. If the Fontainebleau samples used during the experiments are different in grain size or contain earlier formed microscale deformation structures, the compaction creep behavior can be non-comparable for one sample to the other. The samples were cored out of larger size cores, of which we assume they were cored perpendicular to the bedding and parallel to each other. When this assumption is not correct the samples can be heterogeneous and this can result in differences in stress relaxation behavior. Another explanation for the observed results can be that a deformation mechanism other than subcritical cracking controlled creep is active in the Fontainebleau samples, such as grain rearrangements or compaction band formation. To test for this hypothesis the load-up curves of the Bentheim and Fontainebleau experiments were compared. If compaction bands or grain rearrangements would be active during the load-up, the load-up curve would be curved concave up. The load-up curves for all performed experiments are linear, which rules out possible effects of deformation mechanisms such as compaction banding. The active deformation mechanism remains unclear.

The non-consistent results of the Fontainebleau can possibly be explained by heterogeneity of the Fontainebleau samples. The Fontainebleau experiments are unresolved and further research is required for investigation of the effect of chemically active pore fluids on the stress relaxation behavior.

5. Conclusions

Compaction creep and stress relaxation experiments were performed on sand aggregates and sandstone cylinders, respectively. The following conclusions could be drawn:

1) By comparison with previous work, subcritical crack growth by stress corrosion cracking is the major mechanism controlling compaction creep.
2) Compaction creep is inhibited both by the presence of aluminium chloride and by the presence of saturated silica solution. It is enhanced by sodium chloride and by sodium sulfate solution as pore fluid. The inhibiting effects of aluminium chloride on compaction creep are proven to occur in Beaujean sand aggregates and Bentheim sandstone cylinders.
3) The rate of microcracking depends on the pH of the pore fluid. The rate of microcracking is lowest in acidic solutions having a pH near 2. Rates increase with increasing solution pH. Microcracking dependence on pH can explain the inhibiting effect of aluminium chloride solution only, but not the effects of sodium chloride and sodium sulfate.
4) The chemical controls on subcritical crack growth and quartz dissolution and dissolution rate are considered similar. Therefore the effect of aluminium and sodium ions on quartz dissolution are comparable for microcracking in quartz (Dove, 1995). Aluminium and sodium impurities will have opposing effects on dissolution and fracturing of quartz (Iler, 1979; Jephscott and Johnston, 1950; Van Lier, 1965, Dienert and Wandenbulcke, 1923; Dove, 1994). The effect of impurities can explain the observed inhibiting effects of aluminium chloride, and enhancing effects of sodium sulfate and sodium chloride.
5) Quartz solubility and rate of dissolution are inhibited by aluminium impurities. The inhibiting effect of aluminium is caused by chemisorption on the surface of silica (Iler, 1973).
6) Quartz solubility and rate of dissolution are enhanced by sodium atoms. Sodium ions cause weakening and attack of Si-O bonds due to the formation of $\equiv Si - O^{-} Na^{+}$ ion pair surface complexes. Additionally, Na^{+} ions enhance local dissociation of water, causing enhanced attack of the silica surface and rupture of Si-O bonds (Wirth and Gieskes, 1979; Dove, 1994).
7) The Fontainebleau experiments do not show any inhibiting effect of aluminium chloride solution despite that the ultimate stress reached is closer to the failure stress. These experiments require further investigation.

Acknowledgements

I would like to thank my supervisors Prof. Chris Spiers and MSc. Anne Pluymakers: Chris for the opportunity he gave me to do this project, his support, inspiring view, and confidence, and Anne for all the things she taught me, her endless support and criticism. Furthermore, I like to thank the rest of the HPT group, especially Peter van Krieken and Gert Kastelijn for their technical assistance, and Bart

Verberne for his help in performing the experiments. I also thank Ronald Pijnenburg for some interesting discussions and the pleasant work environment.

Appendix I

The measured strain during the experiment is equal to the elastic strain, attained during the experiment by the apparatus and the sample, plus the permanent strain, attained by the sandstone sample. This is represented by Formula (1):

(1) $\varepsilon_M = \varepsilon_P + \varepsilon_E$

Where ε_M is the total measured strain during the experiment, and where ε_P and ε_E are the permanent strain attained by the sandstone sample and the elastic strain attained by the apparatus and the sample together, respectively. By differentiating ε over time Formula (1) could be rewritten into:

(2) $\dot{\varepsilon}_M = \dot{\varepsilon}_P + \dot{\varepsilon}_E$

Where $\dot{\varepsilon}_M$ is the total measured strain rate, and where $\dot{\varepsilon}_P$ and $\dot{\varepsilon}_E$ are the permanent strain rate and elastic strain rate respectively. The elastic portion of the strain rate, so $\dot{\varepsilon}_E$, could be rewritten into Formula (3):

(3) $\dot{\varepsilon}_E = \dot{\sigma}(C_{sample} + C_{apparatus})$

Where $\dot{\sigma}$ is the rate of change of stress and C_{sample} and $C_{apparatus}$ are the compliances of the sample and apparatus respectively. Rewriting Formula (2) and inserting (3) into (2) Formula (2) could now be rewritten into:

(4) $\dot{\varepsilon}_P = \dot{\varepsilon}_M - \dot{\varepsilon}_E$

(5) $\dot{\varepsilon}_P = \dot{\varepsilon}_M - \dot{\sigma}(C_{sample} + C_{apparatus})$

The total measured strain (ε_M) during the experiment is determined by dividing the uncorrected displacement data over the initial sample length. The total strain rate ($\dot{\varepsilon}_M$) is the derivative of strain over time. The rate of change of stress ($\dot{\sigma}$) is the derivative of stress over time after stopping the loading ram (at a load of 85 kN). The compliance of both sample (C_{sample}) and apparatus ($C_{apparatus}$) were derived from the loading curve. The Young's modulus (E) of the experimental setup is load divided by strain ($E = \sigma/\varepsilon$). Young's modulus of the entire set-up and compliance of the sample plus the apparatus can be decribed by the following formula:

(6) $1/E = C_{sample} + C_{apparatus}$

Combining formula 5 and 6 gives the strain rate of the sample, $\dot{\varepsilon}_P$.

(7) $\dot{\varepsilon}_P = \dot{\varepsilon}_M - \dot{\sigma}(1/E)$

References

Atkinson, B.K. (1987), Fracture mechanics of rock (Academic Press geology series), Academic Press Inc., London.

Atkinson, B.K. (1984), Subcritical crack growth in geological matters, *J. Geophys. Res., 89, B6*, 4077-4114.

Brzesowsky, R.H. (1995), Micromechanics of sand grain failure and sand compaction, Ph.D. thesis, 180 pp, Utrecht University, Utrecht.

Chester, F.M., et al. (2007), Subcritical creep compaction of quartz sand at diagenetic conditions: Effect of water and grain size, *J. Geophys. Res., 112*, B06203.

De Waal, J.A. and Smits, R.M.M. (1988), Prediction of reservoir compaction and surface subsidence: Field application of a new model, *SPE Formation Evaluation,* 347-356.

De Waal, J.A. and Smits, R.M.M. (1988), A comparison between the pressure-lag model and the rate-type model for prediction of reservoir compaction and surface subsidence, *SPE Formation Evaluation*, 357-363.

Dienert, F. and Wandenbulcke, W. (1923) *C.R. Acad. Sci*., 176, 1478.

Dove, P. (1995), Geochemical controls on the kinetics of quartz fracture at subcritical tensile stresses, *J. Geophys. Res., 100,* 22,349-22,359.

Fisher, Q.J. et al. (1999), Mechanical compaction of deeply buried sandstones of the North Sea, *Mar. Petr. Geol., 16,* 605-618.

Hangx, S.J.T. et al. (2010), Creep of simulated reservoir sands and coupled chemical-mechanical effects of CO_2 injection, *J. Geophys. Res., 115,* B09205

Heap, M.J. et al. (2009) Time dependent brittle creep in Darley Dale sandstone, *J. Geophys. Res.,114.*

Hettema, M.H.H. et al. (1998), Production-induced compaction of sandstone reservoirs: The strong influence of field stress, *SPE Petroleum Conference, 50630*

Iler, R.K. (1973), Effect of adsorbed alumina on the solubility of amorphous silica in water, *J. Coll. Interf. Sc., 43, 2,* 399-408.

Iler, R.K. (1979), The chemistry of silica: Solubility, polymerization, colloid and surface properties, and biochemistry, John Wiley & Sons, New York.

Jepcott, C.M. and Johnston, J.H. (1950), *Arch. Ind. Hyg. Occup*. Med., 1, 323.

Karner, S. L., et al. (2005), Laboratory deformation of granular quartz sand: Implications for the burial of clastic rocks, AAPG Bull., 89, 603–625.

Klein, E., et al. (2000), Mechanical behaviour and failure mode of Bentheim sandstone under triaxial compression, *Phys. Chem. Earth (A), 26, No 1-2,* 21-25.

Lasaga, A.C. and Gibbs, G.V. (1990), Ab-initio quantum mechanical calculations of water-rock interactions: adsorption and hydrolysis reactions, *American Cer. Soc., 71, 2,* 106-112.

Liteanu, E. and Spiers, C.J. (2009), Influence of pore fluid salt content on compaction creep of calcite aggregates in the presence of subcritical CO_2, *Chem. Geol., 265*, 134-147.

Ngwenya, B.T. et al. (2001), A constitutive law for low-temperature creep of water saturated sandstones, *J. Geophys. Res., 106,* 21,811-21,826.

Niemeijer, A.R. and Spiers, C.J. (2002), Compaction creep of quartz-muscovite mixtures at 500°C: Preliminary results on the influence of muscovite on pressure solution, In: S. de Meer, M.R. Drury, J.H.P. de Bresser and G.M. Pennock (Editors), Deformation Mechanisms, Rheology and Tectonics. Special Publication. Geological Society of London, Noordwijk, pp. 61-72.

Renshaw, C.E., and Pollard, D.D. (1994), Numerical simulation of fracture set formation: A fracture mechanics model consistent with experimental observations, *J. Geophys. Res., 99*, 9359-9372.

Rutter, E.H. and Mainprice, D.H. (1978), The effect of water on stress relaxation of faulted and unfaulted sandstone, *Pageoph, 116,* 634-654.

Sasaki, B. (1952), *Bull. Chem. Res. Inst. Non-aqueous solutions*, Tohoko Univ., 2, 113.

Schutjens, P.M.T.M. (1991), Experimental compaction of quartz sand at low effective stress and temperature conditions, *J. Geol. Soc. London, 148,* 527-539.

Schutjens, P.M.T.M. et al. (2004), Compaction-induced porosity/permeability reduction in sandstone reservoirs: Data and model for elasticity-dominated deformation, *SPE Reservoir Evaluation & Engineering,* 202-216.

Seto, M. et al. (1997) Effect of chemical additives on the strength of sandstone, *Int. J. Rock Mech. & Min. Sci., 34:3-4.*

Sulem, J. et al. (2006) Hydromechanical Behaviour of Fontainebleau sandstone, *Rock Mech. Rock Engng., 39*, 185-213.

Van Lier, J.A. (1965), The solubility of Quartz, Drukkerij en Uitgeverij v/h Kemink en Zoon, n.v. Domplein, Utrecht, Netherlands.

Wirth, G.S. and Gieskes, J.M. (1979), The initial kinetics of the dissolution of vitreous silica in aqueous media. *J. Coll. Interf. Sc., 68, 3,* 492-500.